3.3.2. Cal-Sil Samples

Test #3 was the first ICET test that included cal-sil in addition to fiberglass samples. XRD/XRF results show the crystal structure and the chemical composition of the unused raw and unused baked cal-sil samples. Based on XRD results, both unused raw and unused baked cal-sil samples contained crystalline substances of tobermorite ($Ca_{2.25}(Si_3O_{7.5}(OH)_{1.5})(H_2O)$) and calcite ($CaCO_3$). XRF results indicated that the dominant elemental compositions of cal-sil include Si and Ca and small amount of Al, Fe, Na, and Mg. There was no significant difference in elemental composition between raw and baked unused cal-sil. After being baked in a laboratory oven at 260°C for 72 hours, the raw cal-sil color changed from yellow to pink. The possible property changes of cal-sil after being baked include loss of water and oxidation of reductive species such as organic carbon, Fe(0), and Fe(II), as well as possible mineral and crystal structural changes. Specifically, oxidation of Fe(0) and Fe(II) into Fe_2O_3 is likely responsible for the baked cal-sil's turning pink.

ESEM/SEM/EDS examined a Day-30 unbaked cal-sil sample that had been submerged in the birdcage and a Day-30 baked cal-sil sample that had been submerged in the high-flow zone. EDS results show a significant amount of P on the exterior of the submerged cal-sil samples, both baked and unbaked; almost no P was present in the interior of the submerged cal-sil. (The interior cal-sil sample was obtained by breaking a chunk of cal-sil in half, and the interior sample was examined with SEM.) This result may be explained by the cal-sil exterior surface's being exposed to the testing solution, likely causing phosphate to complex with Ca at the exterior surface. However, because of limited phosphate diffusion into the cal-sil interior, no P was found in the interior cal-sil samples. In addition, unlike fiberglass, cal-sil is granular, making it difficult to distinguish cal-sil particles from the foreign deposits/debris attached on the cal-sil samples. Appendix H includes ESEM and SEM/EDS data for the cal-sil.

3.4. Metallic and Concrete Samples

3.4.1. Weights and Visual Descriptions

3.4.1.1. Submerged Coupons

Examination of the 40 submerged coupons provides valuable insight into the nature of the chemical kinetics that occurred during this 30-day test. The physical change that these coupons experienced is determined through both visual evidence and weight measurement of each coupon before and after the test. Pre-test pictures were taken of the coupons when they were received and before insertion in the racks. Post-test pictures were taken several days after the racks had been removed from the tank. All racks with coupons still inserted were staged to allow complete drying of the coupons before the post-test pictures. The coupons were placed in a low-humidity room and allowed to air dry. All coupons were also weighed before they were inserted into the tank and after the 30-day test was completed. Generally, the submerged coupons experienced more dramatic changes in both appearance and weight.

There are three submerged aluminum coupons in each test. Figures 3-80 through 3-85 display the pre- and post-test pictures of those coupons that were in Test #3. Each post-test aluminum coupon exhibits a pattern of white particulate deposition. In addition, each post-test coupon is a light reddish-brown, which may be attributable to copper's leaching into the test solution. The particulate deposition patterns for post-test aluminum coupons 155 and 156 are similar. However, the deposition pattern for the post-test Al-157 possesses a grayish tint, and a stream of white deposition runs from the rack contact point at the top to the bottom of the coupon. The relative spatial location of these coupons, given in order from the west side of the tank to the east side of the tank, is as follows: Al-155, Al-156, and Al-157. The concentration of particles increases slightly from the western-most coupon to the eastern-most coupon.

Figure 3-80. Al-155, submerged, pre-test.

Figure 3-81. Al-155, submerged, post-test.

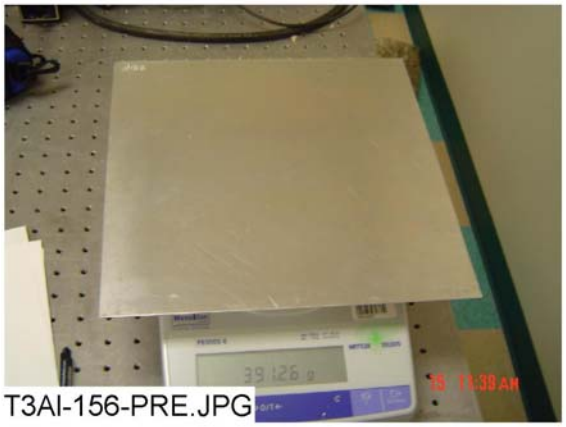

Figure 3-82. Al-156, submerged, pre-test.

Figure 3-83. Al-156 submerged, post-test.

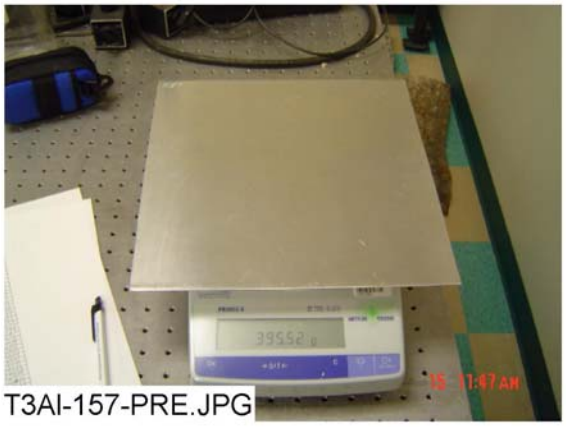

Figure 3-84. Al-157, submerged, pre-test.

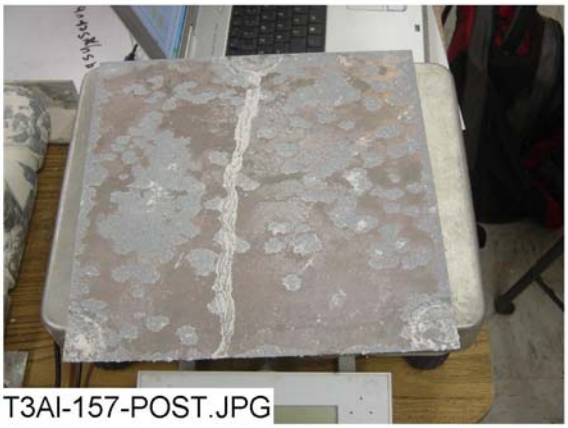

Figure 3-85. Al-157, submerged, post-test.

The galvanized steel coupons exhibited nearly identical patterns of dense gray particle deposition. Figures 3-86 and 3-87 present the pre- and post-test pictures of one submerged galvanized steel coupon. There were no observable differences in post-test appearance based on the coupon's location in the rack.

Figure 3-86. GS-468, submerged, pre-test.

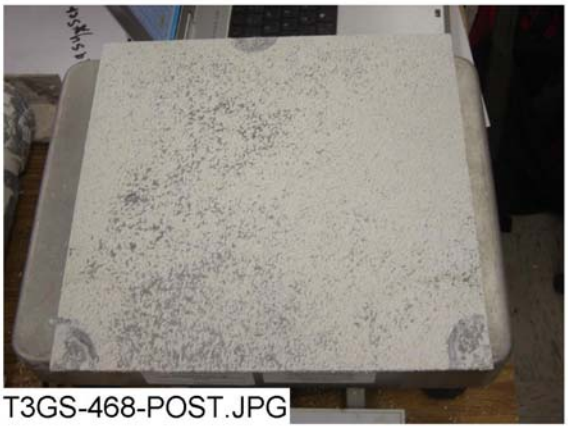

Figure 3-87. GS-468, submerged, post-test.

Figures 3-88 and 3-89 present the pre- and post-test pictures of a typical submerged IOZ-coated steel coupon. Each post-test coated steel coupon exhibited a similar pattern of white particle deposition.

Figure 3-88. IOZ-156, submerged, pre-test.

Figure 3-89. IOZ-156, submerged, post-test.

Figures 3-90 through 3-93 present the pre- and post-test pictures of two submerged copper coupons. The patterns of white deposition are different for these post-test coupons. The CU-207 post-test coupon is almost completely covered with a dense collection of white deposits. The CU-225 post-test coupon, in contrast, exhibits faint horizontal streak-lines of white deposits. The CU-207 coupon was located on the west side of the tank in relation to the CU-225 coupon. The CU-207 coupon gained 1.2 g, while the CU-225 coupon lost 0.1 g.

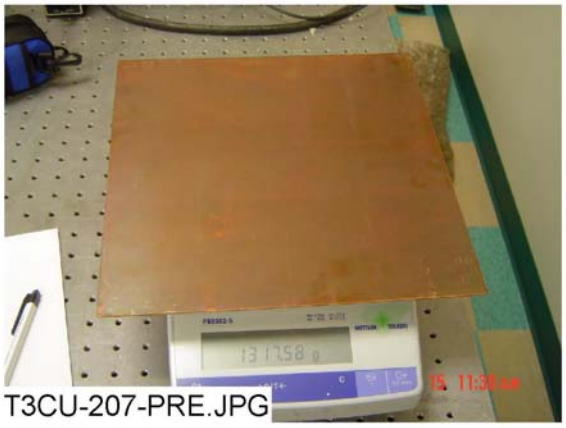

Figure 3-90. CU-207 submerged, pre-test.

Figure 3-91. CU-207, submerged, post-test.

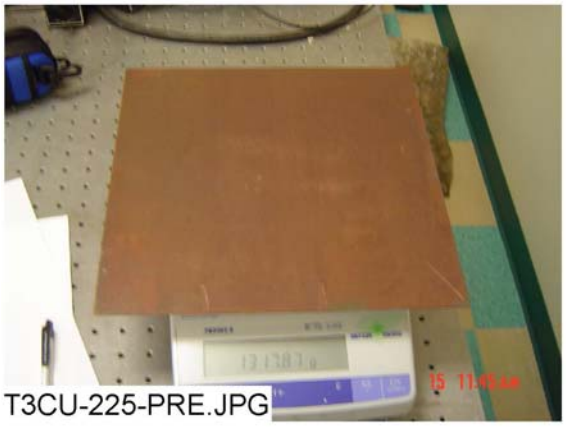

Figure 3-92. CU-225, submerged, pre-test.

Figure 3-93. CU-225, submerged, post-test.

Figures 3-94 and 3-95 present the pre- and post-test pictures of the single submerged carbon steel coupon. It has a light coating of white deposits over a large portion of the surface area. Also, there is observable rust along the bottom edge of the coupon. The rust deposits are mainly congregated near the lower corners of the coupon, near the rack's contact points. Differences in corrosion or deposits at the location of the coupon rack contact points may have been due to stagnant solution conditions that may have limited mass transfer to or from the surface and caused local differences in solution composition. Coupon US-11 lost 1.1 g.

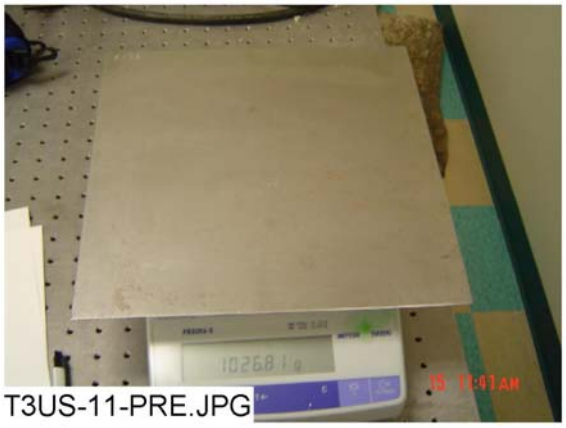

Figure 3-94. US-11, submerged, pre-test.

Figure 3-95. US-11, submerged, post-test.

Figures 3-96 and 3-97 present the pre- and post-test pictures of the submerged concrete coupon. The post-test concrete coupon exhibits an enhanced gray compared with the pre-test coupon. The concrete coupon gained 180.5 g, which is estimated to be primarily water absorption.

Figure 3-96. Conc-005, submerged, pre-test.

Figure 3-97. Conc-005, submerged, post-test.

Table 3-2 presents the pre- and post-test weight data for each representative submerged coupon shown above.

Table 3-2. Weight Data for Submerged Coupons

Type	Coupon No.	Pre-Test Wt. (g)	Post-Test Wt. (g)	Net Gain/Loss
Al	155	393.0	398.7	5.7
Al	156	391.2	392.2	1.0
Al	157	395.5	390.8	-4.7
GS	468	1058.1	1074.0	15.9
IOZ	156	1600.9	1602.4	1.5
CU	207	1317.6	1318.8	1.2
CU	225	1317.9	1317.8	-0.1
US	11	1026.8	1025.7	-1.1
Conc	5	8020.0	8200.5	180.5

Table 3-3 shows the mean weight gain/loss summary in grams for all of the submerged coupons.

Table 3-3. Mean Weight Gain/Loss (g) Data for Submerged Coupons

Coupon Type	Mean Gain - Loss (g)
AL	0.6
GS	15.0
CU	0.3
IOZ	1.8
US	-1.1
Concrete	180.5

3.4.1.2. Unsubmerged Coupons

Compared with the submerged Test #3 coupons, unsubmerged Test #3 coupons were effected less by their 30-day exposure. While they experienced some changes, those changes were far less significant than the changes seen in submerged coupons.

Figures 3-98 and 3-99 show the pre- and post-test pictures of a typical unsubmerged aluminum coupon. The coupons exhibit a light pattern of deposition. Also, each post-test coupon has coarser texture and a less-lustrous surface.

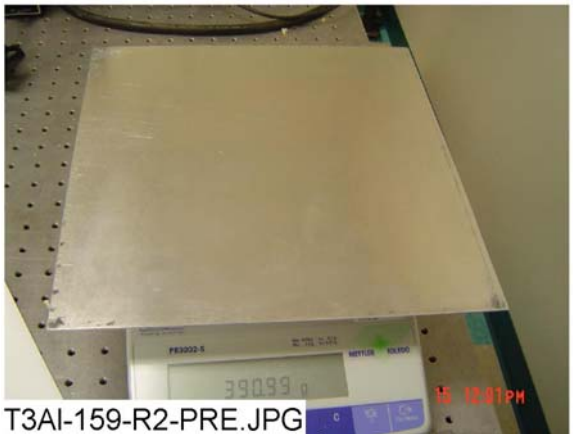

Figure 3-98. Al-159, unsubmerged, pre-test.

Figure 3-99. Al-159, unsubmerged, post-test.

Figures 3-100 and 3-101 show the pre- and post-test pictures of a typical unsubmerged galvanized steel coupon. Each post-test galvanized steel coupon exhibited a similar light deposition.

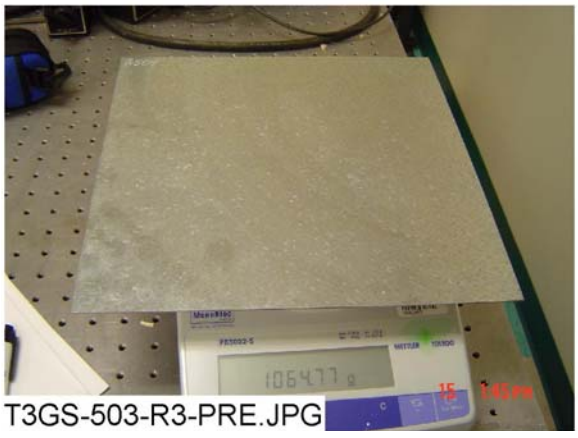

Figure 3-100. GS-503, unsubmerged, pre-test.

Figure 3-101. GS-503, unsubmerged, post-test.

Figures 3-101 and 3-102 present the pre- and post-test pictures of a typical unsubmerged copper coupon. Each post-test copper coupon exhibited a similar pattern of streak-like deposition.

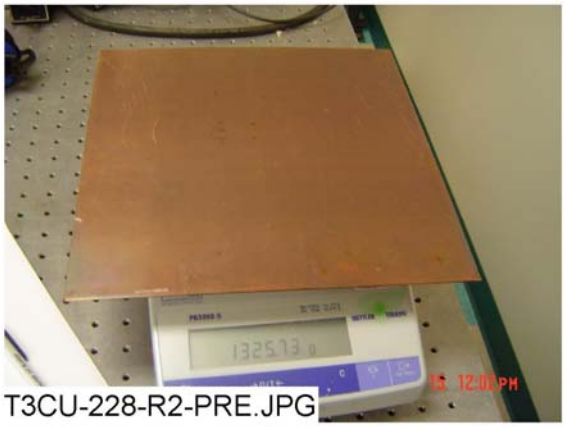

Figure 3-102. CU-228, unsubmerged, pre-test.

Figure 3-103. CU-228 unsubmerged, post-test.

Figures 3-104 and 3-105 present the pre- and post-test pictures of a typical unsubmerged IOZ-coated steel coupon. Each post-test coated steel coupon exhibited a similar pattern of deposition.

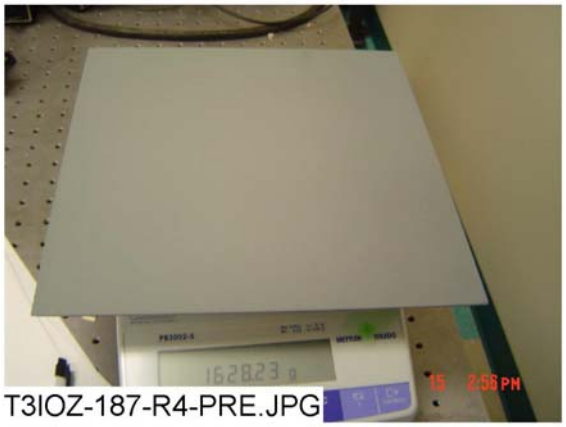

Figure 3-104. IOZ-187, unsubmerged, pre-test.

Figure 3-105. IOZ-187, unsubmerged, post-test.

Figures 3-106 and 3-107 present the pre- and post-test pictures of a typical unsubmerged carbon steel coupon. The post-test carbon steel coupons turned reddish-brown and exhibited slight corrosion around the edges.

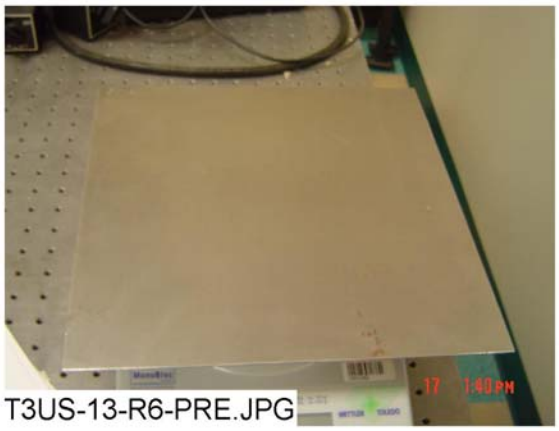

Figure 3-106. US-13, unsubmerged, pre-test.

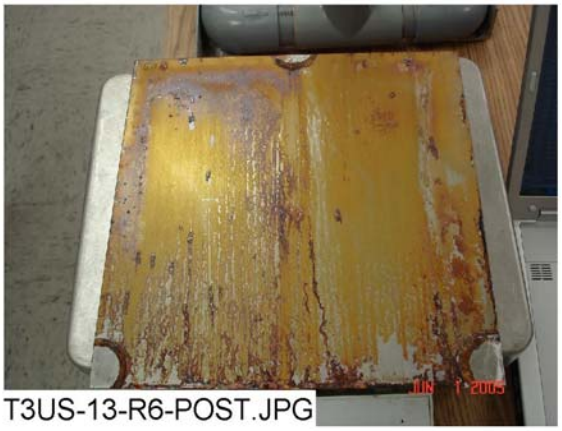

Figure 3-107. US-13, unsubmerged, post-test.

Table 3-4 presents the pre- and post-test weight data for each representative unsubmerged coupon.

Table 3-4. Weight Data for Unsubmerged Coupons

Type	Coupon No.	Pre-Test Wt. (g)	Post-Test Wt. (g)	Net Gain/Loss
Al	159	391.0	391.6	0.6
GS	503	1049.0	1049.1	0.1
IOZ	187	1628.2	1630.4	2.2
CU	228	1325.7	1325.7	0.0
US	13	1023.2	1023.7	0.5

Table 3-5 presents the mean weight gain/loss summary in grams for all of the unsubmerged coupons.

Table 3-5. Mean Gain/Loss (g) Data for Unsubmerged Coupons

	Mean Gain-Loss Per Coupon Type (g)				
Rack	AL	GS	CU	IOZ	US
2	0.5	0.1	0.3	1.6	n/a
3	0.0	0.1	0.0	1.4	n/a
4	0.2	0.3	0.0	2.1	1.4
5	0.6	0.1	0.1	2.4	n/a
6	0.6	0.3	0.3	2.3	0.5
7	0.4	0.1	0.3	2.3	n/a
Overall	0.4	0.2	0.2	2.0	1.0

3.4.2. SEM Analyses

3.4.2.1. Submerged Coupons

During the ICET tests, trace metal cations may be released from the submerged metal coupon surfaces due to corrosion effects. Subsequently, the released metal cations may complex with the anions from the solution through electrostatic interactions, resulting in, for example, OH^-, PO_4^{3-}, SiO_3^{2-}, and CO_3^{2-}. In turn, the complexated anions may attract other cations from the solution, such as Ca^{2+}, Mg^{2+}, Al^{3+}, Cu^{2+}, Zn^{2+}, and H^+. As a result, corrosion products (deposits) are formed and may continuously grow on the metal coupon surfaces. The thickness of the deposits is in the millimeter range. The adherence between the metal coupons and the deposits is through chemical bonds, which are a much stronger connection than van der Waals forces. Due to the vertical placement of the metal coupons in the tank (with a small horizontal cross-sectional area), the deposits on the metal coupon surface are likely of chemical origin rather than being the result of particles settling on the surface.

According to SEM/EDS results, the dominant corrosion products on the submerged Al coupons are likely aluminum hydroxide with other substances containing Si, Ca, and O. For submerged Cu coupons, the possible corrosion products include CuO, $Cu_2(CO_3)(OH)_2$, and substances containing Ca, Si, and O. For the submerged galvanized steel coupons, the possible corrosion products are phosphate, silicate, and carbonate compounds of Zn and Ca. For the submerged steel coupons, the possible corrosion products include phosphate, silicate, and carbonate compounds of Fe and Ca and compounds composed of Fe, Al, Si, Ca, P, and O.

3.4.2.2. Unsubmerged Coupons

The physical and chemical changes that the unsubmerged coupons experienced during Test #3 are less significant than the changes seen on the submerged coupons. The unsubmerged coupons were affected by the testing solution only during the 4-hour spraying period on the first day of the test and, following that, were affected by water vapor throughout the test.

According to SEM/EDS results, the dominant corrosion products on the unsubmerged Al coupons are likely aluminum hydroxide and/or aluminum oxide. For unsubmerged Cu, the corrosion products on the coupon surface are likely CuO and $Cu_2(CO_3)(OH)_2$. ZnO and $ZnCO_3$ are likely the dominant corrosion products on the unsubmerged galvanized steel coupon surface. For the unsubmerged steel coupon, the likely corrosion products are Fe_2O_3, $Fe(OH)_3$, and $Fe_2(CO_3)_3$.

Appendix E contains the SEM data for the coupons.

3.5. Sedimentation

Sediment was collected from the tank bottom after the test solution was drained. It consisted of two main macroscopic quantities, a particulate sediment on the bottom covered in many places with a whitish-pink gel-like material. Figure 3-108 shows this sediment. In addition, Figure 3-109 shows SS mesh holding insulation samples after it was pulled from the tank bottom. The pink and yellow particulate sediment covers much of the mesh, and the gel-like material is seen above it and is being pointed to in the figure.

The particulate sediment samples were identified and classified by their color: pink or yellow. The yellow or pink sediments were large enough (pea-sized or larger) to be visually seen and picked up from the bulk sediment. The pink sediment likely originated from baked cal-sil debris and the yellow sediment from unbaked cal-sil debris. ESEM/EDS and XRD/XRF analysis provided the information on the morphology and composition of these sediments. EDS results show that there is no significant compositional difference between the yellow and pink sediments. Both contain significant amounts of Si, Ca, and O. XRF results consistently show that Si and Ca are the major elements in the mixed sediments. However, P (present in phosphorus pentoxide, P_2O_5) is less than 2% of the total mass, possibly because Test #3 precipitates containing P make up a smaller portion of the total debris than do particles originating from cal-sil.

Based on XRD results, a sediment sample recovered from the bottom of the test tank contained crystalline substances of tobermorite ($Ca_{2.25}(Si_3O_{7.5}(OH)_{1.5})(H_2O)$) and calcite ($CaCO_3$), which are the same as unused baked or unbaked cal-sil samples. XRD results are consistent with the ESEM/EDS analysis, i.e., most of the sediments in the test tank were generated from the baked and unbaked cal-sil debris. However, other debris such as corrosion products, white gel-like precipitates, and fiberglass may also contribute to the sediments. Figures 3-110 through 3-117 and Table 3-6 provide ESEM/EDS and XRD/XRF analysis results. A comparison of Figures 3-113 and 3-114 shows that the surface morphology of the deposits was consistent even in locations where the thickness or ruggedness of the deposits varied. The complete Day-30 sediment analysis is contained in Appendix I.

Figure 3-108. Sediment removed from the tank. Some gel appears on the top.

Figure 3-109. Samples removed from the tank bottom.

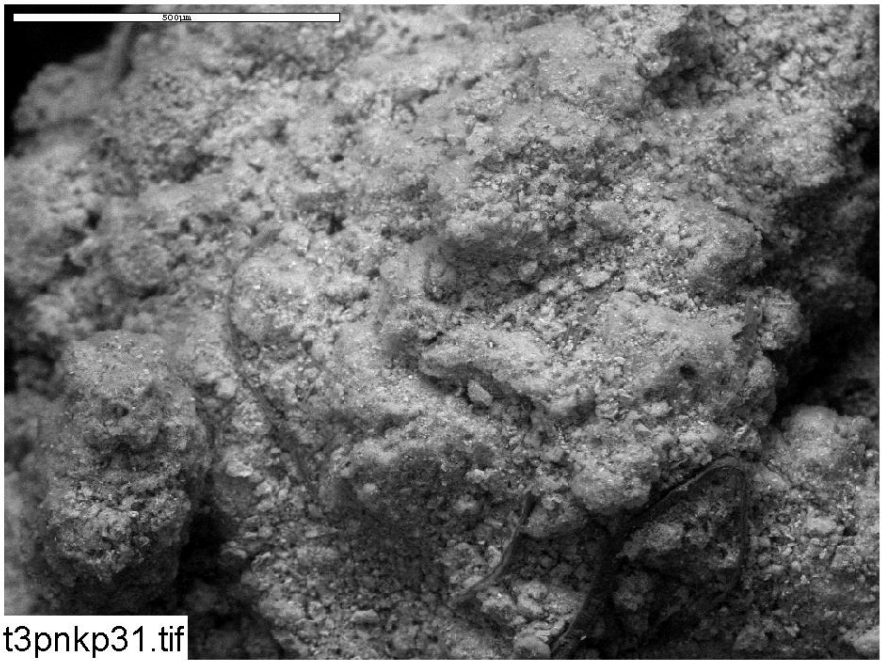

Figure 3-110. ESEM image of a Test #3, Day-30 pink sediment, magnified 100 times. (t3pnkp31, 5/6/05)

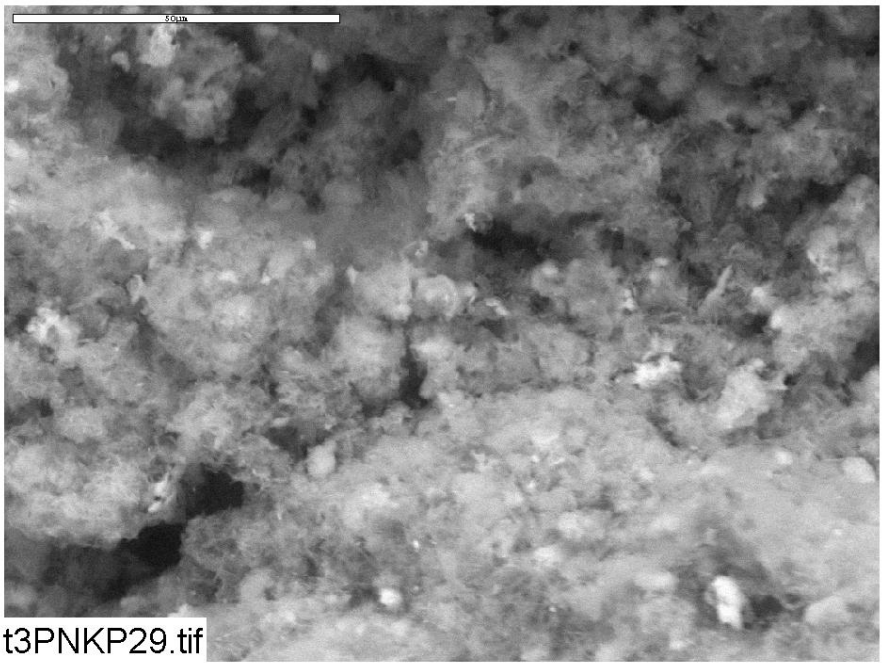

Table 3-111. ESEM image of a Test #3, Day-30 pink sediment, magnified 1000 times. (t3PNKP29, 5/6/05)

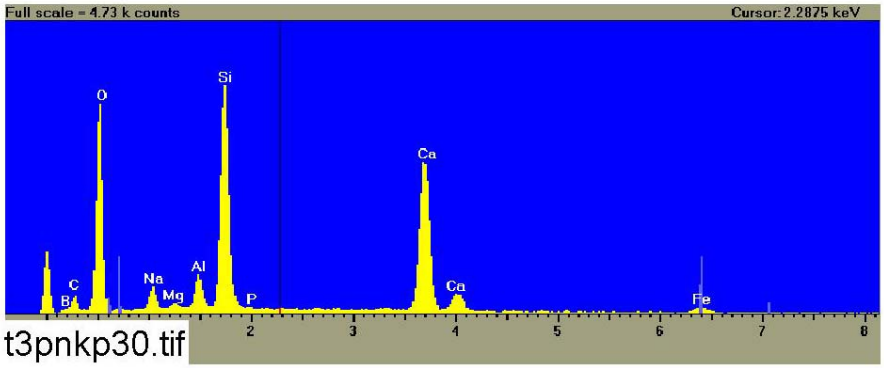

Table 3-112. EDS counting spectrum for the sediment shown in Figure 3-111. (t3pnkp30, 5/6/05)

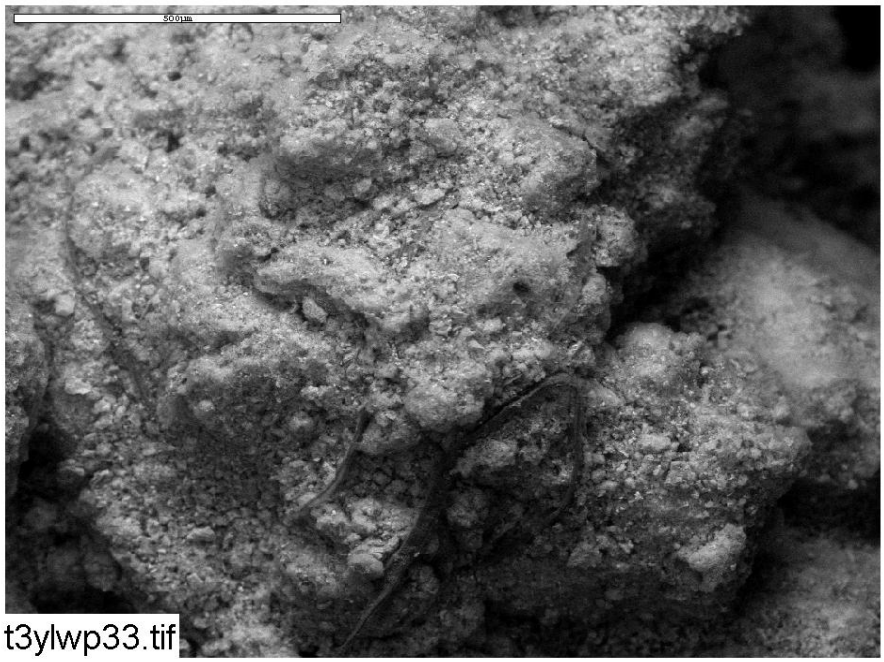

Figure 3-113. ESEM image of a Test #3, Day-30 yellow sediment, magnified 100 times. (t3ylwp33, 5/6/05)

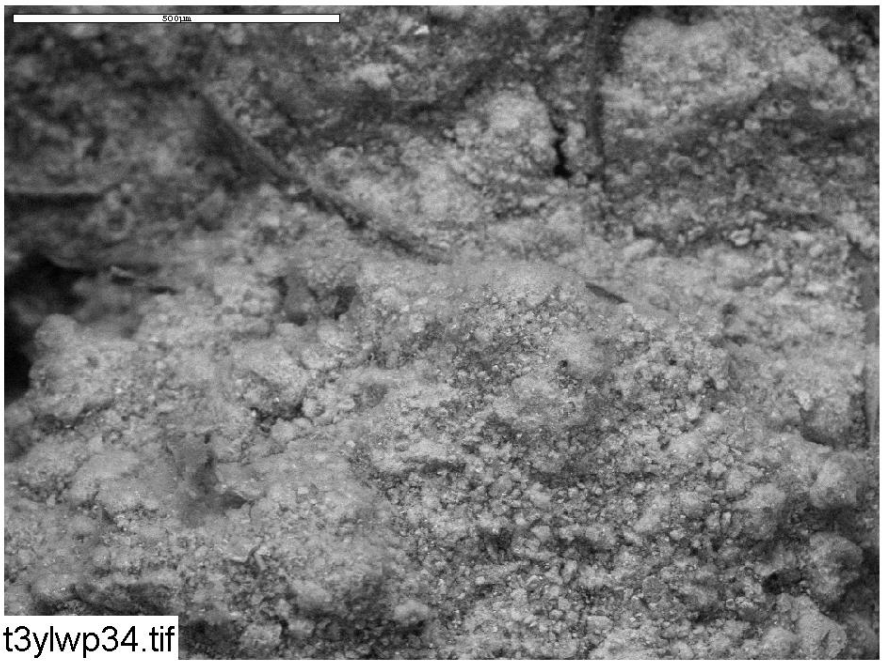

Figure 3-114. ESEM image of a Test #3, Day-30 yellow sediment, magnified 100 times. (t3ylwp34, 5/6/05)

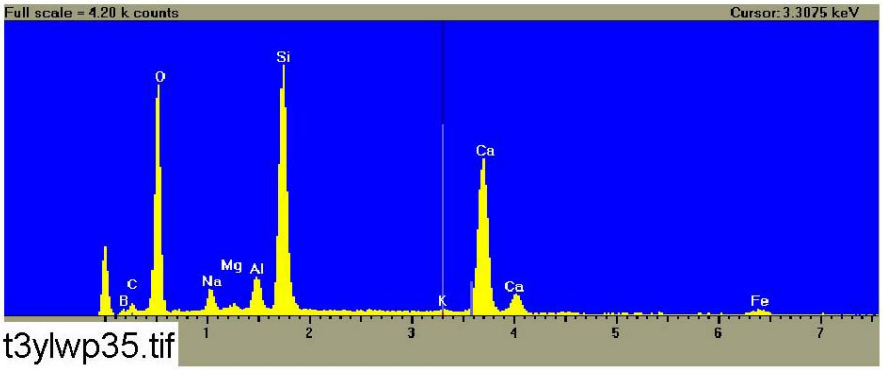

Figure 3-115. EDS counting spectrum for the particles shown in Figure 3-114. (t3ylwp35, 5/6/05)

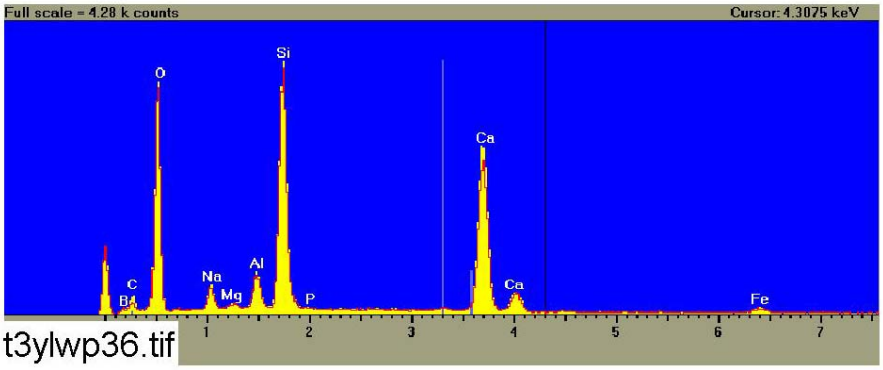

Figure 3-116. Comparison of EDS counting spectra for pink sediment (yellow, t3pnkp30) and yellow sediment (red, t3ylwp35). (t3ylwp36, 5/6/05)

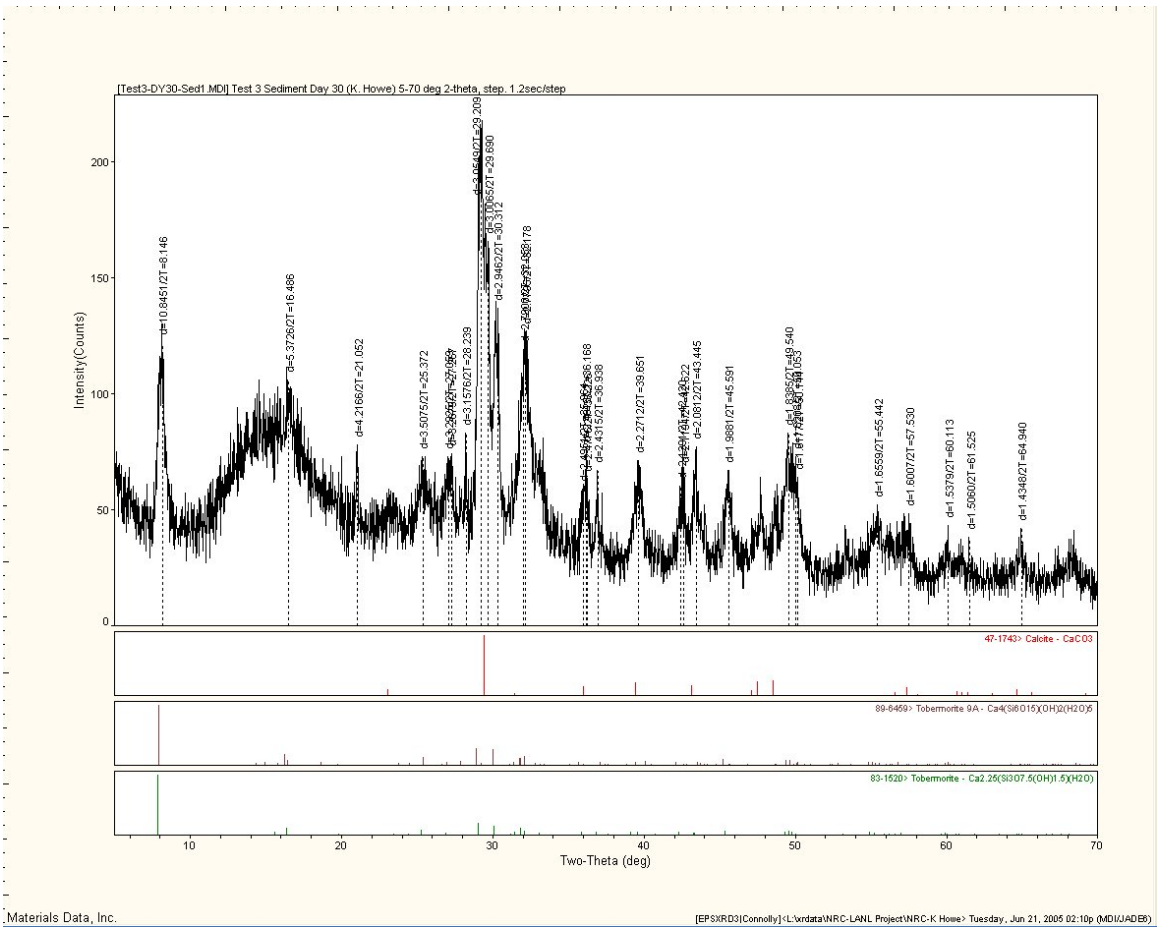

Figure 3-117. XRD results for Test #3, Day-30 mixed sediment.

Table 3-6. Dry Mass Compositions of Test #3, Day-30 Sediment by XRF Analysis

The first row is the chemical component; the second row is the mass composition (%).														
SiO_2	**TiO_2**	**Al_2O_3**	**Fe_2O_3**	**FeO**	**MnO**	**MgO**	**CaO**	**Na_2O**	**K_2O**	**$H_20(-)$**	**$H_2O(+)CO_2$**	**P_2O_5**	**Total**	**$H_2O(+)CO_2$ /DF (10) & Cover. To %**
36.29	0.20	4.92	2.24	0.00	0.06	0.62	27.16	2.19	0.45	0.58	20.65	3.05	98.42	1.0211

3.6. Precipitates

Test #3 was markedly different from Test #1 in that no precipitate was found in the test solution, even after it cooled to room temperature. Based on a series of bench-top controlled experiments, the white precipitate observed in Test #1 contained a significant amount of aluminum. The aluminum concentration of the Test #1 solution was as high as 350 mg/L. However, the aluminum in the Test #3 solution occurred only in trace amounts.

3.7. Corrosion Products

Powder samples were collected from five different locations in the tank on Day 30. These samples included (1) fine powders on a piece of the submerged chlorinated polyvinyl chloride [CPVC] rack, (2) corrosion products on a submerged galvanized steel coupon, (3) corrosion products on a submerged copper coupon, (4) corrosion products on a submerged aluminum coupon, and (5) corrosion products on the submerged concrete coupon.

These corrosion products were collected by directly adhering onto double-sided carbon tape for probe SEM/EDS examination. After the samples were dried in air, Au/Pd coating was applied to enhance the surface conductivity for SEM examination. ESEM and SEM/EDS results indicated that the fine powders collected from the submerged CPVC rack are composed mainly of O, Ca, and P, which make up 95% of the composition of the powder. Therefore, the powders are likely $Ca_3(PO_4)_2$, which precipitated out of the testing solution and became sediment on the submerged rack. The corrosion products collected from the submerged galvanized steel coupon are composed mainly of O, Zn, Si, and Ca. The possible substances are silicate compounds of Zn and Ca. The corrosion products on the surface of the submerged copper coupon are rich in O, Ca, P, and Si. Therefore, they are likely phosphate and silicate compounds of Ca. The corrosion products on the surface of the submerged aluminum coupon are composed mainly of O, Si, Al, Ca, and B. As a result, the possible substances include silicate and boric compounds of Al and Ca. The corrosion/reaction products on the submerged concrete coupon are rich in Ca, O, P, and Si. So, they are likely phosphate and silicate compounds of Ca.

It should be noted that the corrosion/reaction products analysis is not exactly the same as the coupon surface examination because the corrosion/reaction products reflect just the substances on the very top surface of the coupons, while coupon examination gives more details of the compounds on the subsurface and on the coupon itself (see Subsection 3.4).

Appendix D contains the ESEM and SEM/EDS data for the corrosion products.

3.8. Gel Analysis

3.8.1. Visual Description

In ICET Test #3, one significant phenomenon is the presence of white gel-like precipitates in the test solution, especially during and after the injection of TSP on the first day of the test. When Test #3 was shut down, deposits of the pinkish-white gel-like precipitates were observed on the top of the birdcage and on other objects on the tank's bottom. Figures 3-118 and 3-119 show the gel-like precipitates.

Figure 3-118. Gel-like material covering SS mesh on the bottom of the test tank.

Figure 3-119. Gel-like material recovered from the bottom of the test tank.

3.8.2. ESEM and SEM/EDS Analyses

ESEM/SEM/EDS and XRD/XRF analyses were used to characterize the white gel-like precipitates. EDS results show that 92% of the gel-like precipitate is composed of Ca, O, and P. Consistently, XRF results indicate that the gel-like precipitates contain significant amounts of Ca and P. Therefore, it is likely that the white gel-like precipitate is $Ca_3(PO_4)_2$. In addition, EDS and XRF results also indicate that the gel-like precipitates have a small amount of C, which is possibly from carbonate (CO_3^{2-}) and/or organic carbon from the testing solution.

Based on the XRD results, the white gel-like precipitates contained crystalline substances of sodium calcium hydrogen carbonate phosphate hydrate ($Ca_8H_2(PO_4)_6 \cdot H_2O \cdot NaHCO_3 \cdot H_2O$) and lithium calcium hydrogen carbonate phosphate hydrate ($Ca_8H_2(PO_4)_6 \cdot H_2O \cdot Li_2CO_3 \cdot H_2O$). It should be noted that XRD can detect only crystalline substances. If the formed $Ca_3(PO_4)_2$ is amorphous, it cannot be reflected by XRD results.

In Test #3, significant amounts of the white gel-like precipitates were deposited on the top of the birdcage. EDS analysis was performed to compare the white gel-like precipitates on the bottom of the tank with the particulate deposits on exterior fiberglass samples taken from the birdcage. That analysis shows that their compositions are not exactly the same. The gel-like precipitates from the bottom of the tank contain higher amounts of P and lower amounts of Si than do the particulate deposits on samples from the birdcage exterior. This result suggests that some cal-sil debris were deposited on the birdcage exterior in addition to the white gel-like precipitates. As with any SEM sample,

the gel-like precipitates were dried before analyses. Because they were a thick slurry and a mostly solid sample, the drying process is unlikely to affect the major solid composition of the sample. Other precipitates with high P content have chemical similarity with the dried gel-like precipitates.

Figures 3-120 through 3-126, Table 3-7, and Table 3-8 provide SEM/ESEM/EDS and XRD/XRF analysis results. The complete set of Day-30 gel analyses is contained in Appendix G.

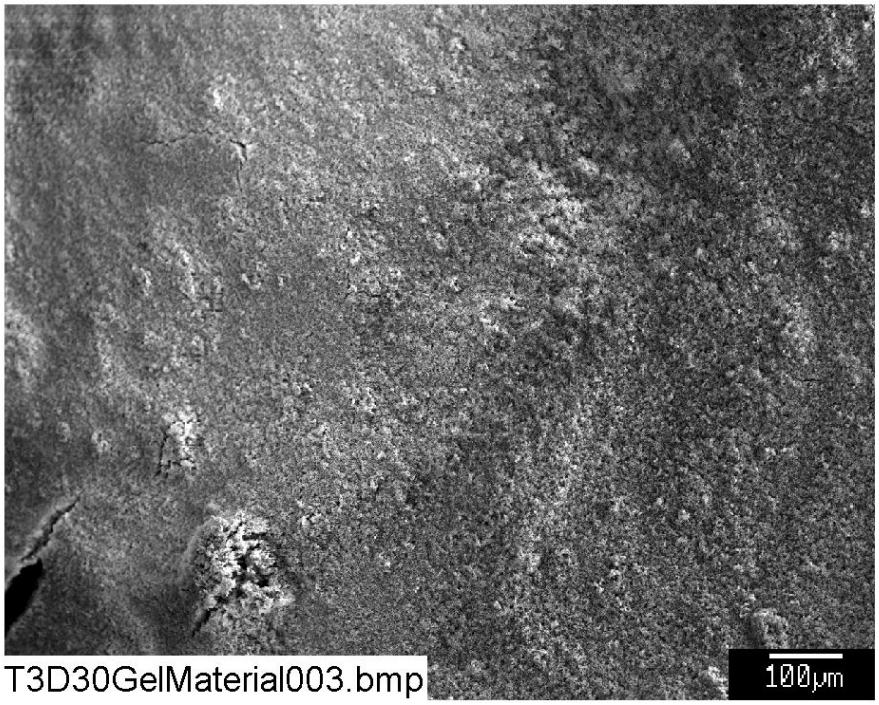

Figure 3-120. SEM image of a Test #3, Day-30 white gel-like material from the top of the birdcage, magnified 100 times. (T3D30GelMaterial003, 5/9/05)

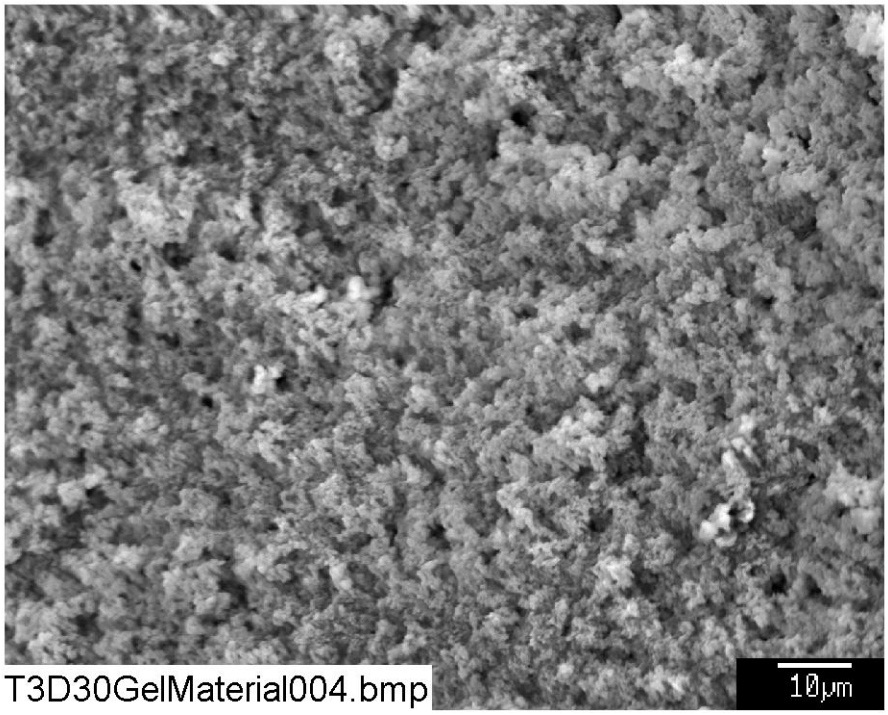

Figure 3-121. SEM image of a Test #3, Day-30 white gel-like material from the top of the birdcage, magnified 1000 times. (T3D30GelMaterial004, 5/9/05)

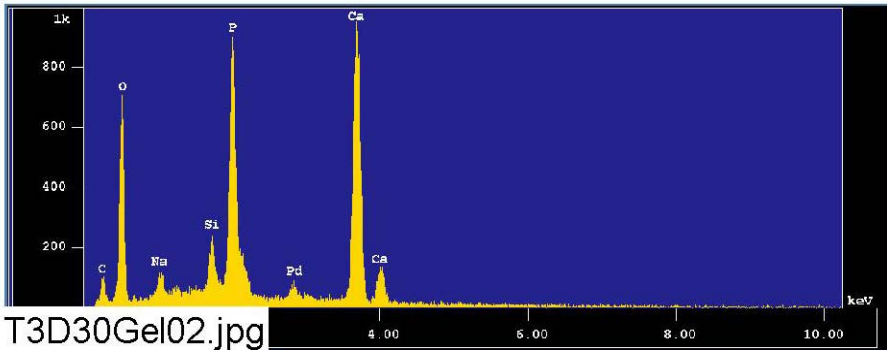

Figure 3-122. EDS counting spectrum for the white, gel-like material (whole image) shown in Figure 3-121. (T3D30Gel02, 5/9/05)

The results from the chemical composition analysis for Figure 3-122 are given in Table 3-7.

Table 3-7. The Chemical Compositions for Figure 3-122

May 9 2005

Group : NRC
Sample : T3D30 ID# : 2
Comment : GelMaterial
Condition : Full Scale : 20KeV(10eV/ch,2Kch)
Live Time : 60.000 sec Aperture # : 1
Acc. Volt : 15.0 KV Probe Current : 1.606E-09 A
Stage Point : X=79.625 Y=59.260 Z=11.424
Acq. Date : Mon May 9 11:42:11 2005

Element	Mode	ROI(KeV)	K-ratio(%)	+/-	Net/Background
C K	Normal	0.09- 0.46	0.6057	0.0005	338 / 119
O K	Normal	0.25- 0.77	12.2043	0.0032	4587 / 68
Na K	Normal	0.81- 1.27	0.5675	0.0010	613 / 50
Si K	Normal	1.50- 2.05	0.9391	0.0005	1366 / 271
P K	Normal	1.75- 2.38	8.4975	0.0055	7628 / 107
Ca K	Normal	3.39- 4.30	17.1295	0.0038	12109 / 26

Chi_square = 42.7915

Element	Mass%	Atomic%	ZAF	Z	A	F
C	4.355	7.8616	3.7318	1.0194	3.6611	0.9999
O	45.521	61.6928	1.9361	0.9721	1.9917	1.0000
Na	1.639	1.5456	1.4989	1.0256	1.4614	1.0000
Si	2.072	1.5994	1.1451	0.9756	1.1812	0.9937
P	13.776	9.6435	0.8415	1.1708	0.7203	0.9978
Ca	32.638	17.6571	0.9890	0.9947	0.9943	1.0000

Total 100.000 100.0000
Normalization factor = 1.9265
Total 100.000 100.0000
Normalization factor = 2.1120

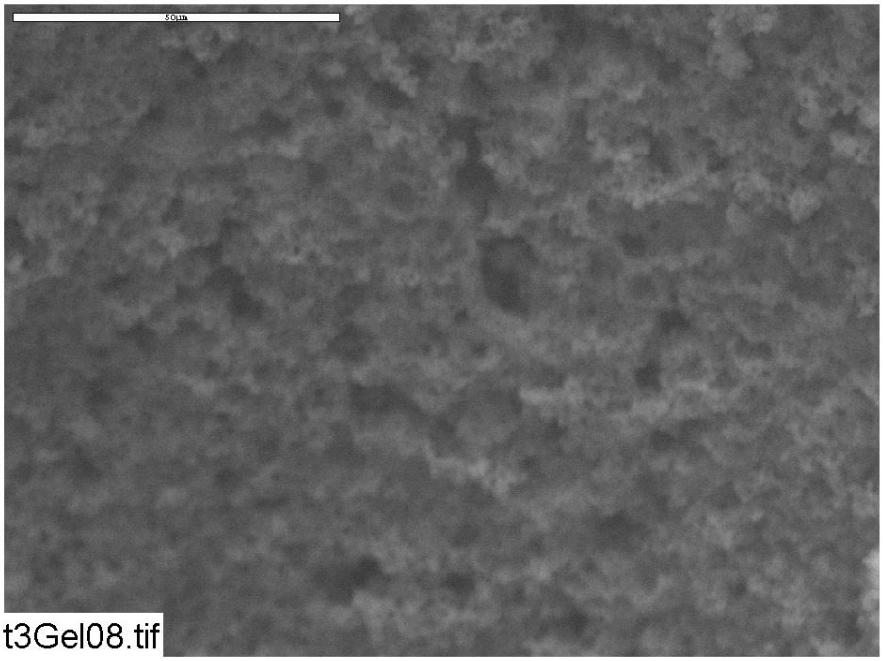

Figure 3-123. ESEM image of a Test #3, Day-30 white gel-like material from the top of the birdcage, magnified 1000 times. (t3Gel08, 5/6/05)

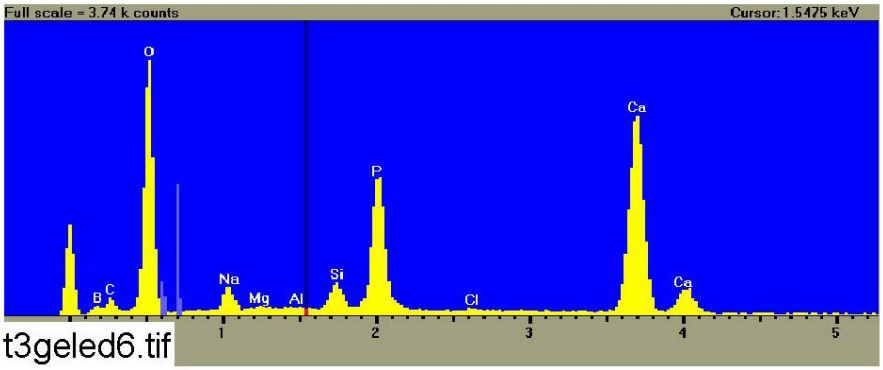

Figure 3-124. EDS counting spectrum for the white, gel-like material shown in Figure 3-123. (t3geled6, 5/6/05)

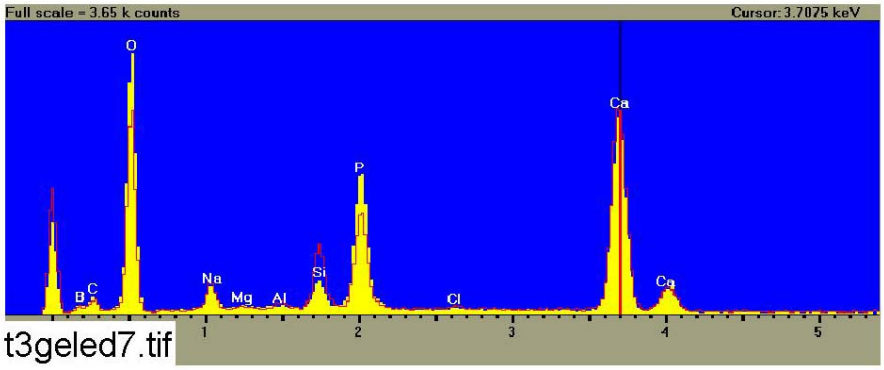

Figure 3-125. Comparison of EDS counting spectra for Figure 3-124 (yellow: the gel-like materials shown in Figure 3-123) and Figure 3-73 (red: the large deposits taken from the birdcage exterior shown in Figure 3-72). (t3geled7, 5/6/05)

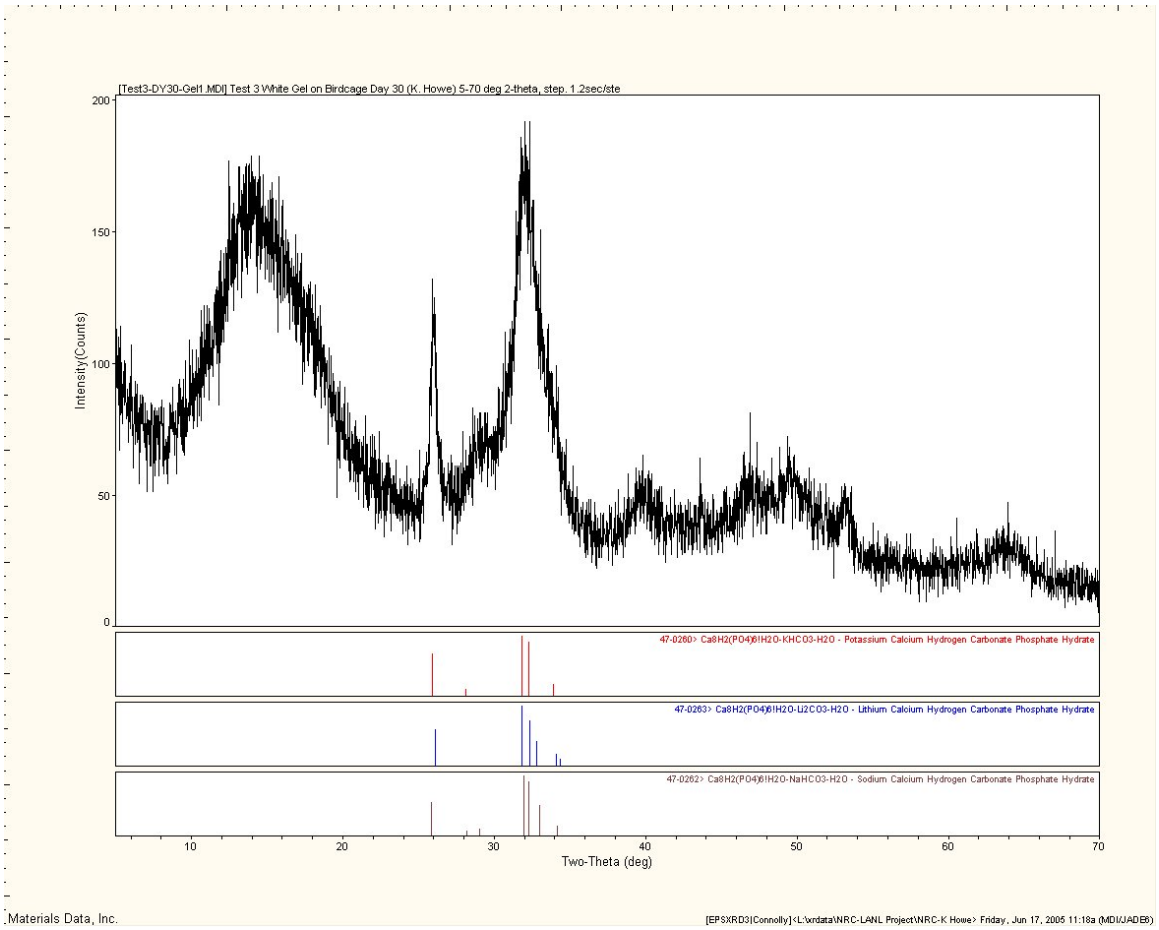

Figure 3-126. XRD results for a Test #3, Day-30 white, gel-like sample.

Table 3-8. Dry Mass Composition of a Test #3, Day-30 White Gel-like Sample by XRF Analysis

The first row is the chemical component; the second row is the mass composition (%).														
SiO_2	**TiO_2**	**Al_2O_3**	**Fe_2O_3**	**FeO**	**MnO**	**MgO**	**CaO**	**Na_2O**	**K_2O**	**$H_20(-)$**	**$H_2O(+)CO_2$**	**P_2O_5**	**Total**	**$H_2O(+)CO_2$ /DF (10) & Cover. To %**
5.26	0.02	0.63	0.07	0.00	0.00	0.25	35.01	2.39	0.06	4.75	19.24	27.09	94.77	1.0196

This page intentionally left blank.

4. SUMMARY OF KEY OBSERVATIONS

ICET Test #3 was conducted successfully, maintaining the critical physical and chemical parameters called out in the Test Plan. The test ran uninterrupted for 30 days. The solution chemistry behaved as expected, with the turbidity declining from its early values to steady numbers from Day 1 until the end of the test. TSS was relatively steady near its baseline value, with some increases during the test. The kinematic viscosity was steady for the entire test; and the pH was steady, averaging a value of 8.0.

Samples of the solution were taken daily. The chemical elements present were calcium, magnesium, silica, and sodium. Aluminum, copper, iron, zinc, and nickel were present in trace amounts. Strain-rate viscosity measurements indicated that the solution remained Newtonian throughout the test. No precipitates were observed in the solution, even after it had cooled to room temperature.

The submerged aluminum, IOZ-coated steel, copper, and uncoated steel coupons developed significant amounts of white particulate deposits. The aluminum coupons gained an average of 0.6 g, the IOZ-coated steel coupons 1.8 g, the copper 0.3 g, and the uncoated steel coupon lost 1.1 g. The submerged galvanized steel coupons were covered with a dense, gray particulate deposition, and they gained an average of 15.0 g.

The unsubmerged coupons exhibited light patterns of deposition, and they all experienced uniform weight gains. The aluminum coupons gained an average of 0.4 g, the galvanized steel 0.2 g, the copper 0.2 g, the IOZ-coated steel 2.0 g, and the uncoated steel 1.0 g.

Deposits on the fiberglass samples increased over time, and the deposits appeared to be chemically originated for the samples not lying on the tank bottom. These deposits covered individual fiberglass strands and in some cases formed webs between strands. Based on the SEM and ESEM results, the deposits likely originated from chemical precipitation during the sample-drying process. Comparing Days 4, 15, and 30 fiberglass samples showed deposits that were similar in property and amount. There was no significant difference in the amount of deposits found in the exterior and interior samples. Deposits found on the drain collar fiberglass were likely physically attached, and the exterior samples had significantly more deposits than the interior samples. Two different deposits were identified with EDS, one with a higher percentage of P and one with a higher percentage of Si. The former is likely calcium phosphate particles and the latter cal-sil particles. Deposits on and in the birdcage fiberglass similarly had the two different particulate deposits present. In addition, a pinkish-white gel-like precipitate covered the birdcage and much of the sediment. This gel had a consistency much like face cream, and it was composed primarily of Ca, O, and P, making it likely calcium phosphate.

Sediment on the tank bottom was prevalent, accumulating to depths of over 8 in. The sediment contained crystalline substances and calcite, making it primarily cal-sil, although some fugitive fiberglass was also present.

REFERENCES

1. “Test Plan: Characterization of Chemical and Corrosion Effects Potentially Occurring inside a PWR Containment Following a LOCA, Rev. 12c,” March 30, 2005.

2. J. Dallman, J. Garcia, B. Letellier, and K. Howe, “Integrated Chemical Effects Tests: Data Compilation for Test 1,” LA-UR-05-0124, July 2005.

3. “Pre-Test Operations, Test #3,” ICET-PI-012, Rev. 1, April 1, 2005.

4. “Test Operations, Test #3 (cal-sil and fiberglass, with TSP),” ICET-PI-014, Rev. 0, April 5, 2005.

5. “Post-Test Operations, Test #3,” ICET-PI-008, Rev. 3, May 2, 2005.